



## Co<sub>3</sub>O<sub>4</sub>–Co<sub>2</sub>ZnO<sub>4</sub> spinels: The case for a solid solution

Nicola H. Perry<sup>a</sup>, Thomas O. Mason<sup>a,\*</sup>, Chengcheng Ma<sup>b</sup>, Alexandra Navrotsky<sup>b</sup>, Yezhou Shi<sup>c</sup>, Joanna S. Bettinger<sup>c</sup>, Michael F. Toney<sup>c</sup>, Tula R. Paudel<sup>d</sup>, Stephan Lany<sup>d</sup>, Alex Zunger<sup>e</sup>

<sup>a</sup> Department of Materials Science and Engineering, Northwestern University, Evanston, IL 60208, USA

<sup>b</sup> Peter A. Rock Thermochemistry Laboratory and NEAT ORU, University of California, Davis, CA 95616, USA

<sup>c</sup> SLAC National Accelerator Laboratory, Menlo Park, CA 94025, USA

<sup>d</sup> National Renewable Energy Laboratory, Golden, CO 80401, USA

<sup>e</sup> University of Colorado, Boulder, CO 80309, USA

### ARTICLE INFO

#### Article history:

Received 30 December 2011

Received in revised form

8 February 2012

Accepted 9 February 2012

Available online 18 February 2012

#### Keywords:

Co<sub>3</sub>O<sub>4</sub>

ZnCo<sub>2</sub>O<sub>4</sub>

Calorimetry

Diffraction

Mixing thermodynamics

Electrical conductivity

### ABSTRACT

In prior first-principles theoretical work we predicted a complete solid solution in the Co<sub>3</sub>O<sub>4</sub>–Co<sub>2</sub>ZnO<sub>4</sub> system, with a negligibly small mixing enthalpy. In this work we tested this prediction on bulk, large-grained specimens across the Co<sub>3</sub>O<sub>4</sub>–Co<sub>2</sub>ZnO<sub>4</sub> join, combining oxide melt solution calorimetry, differential scanning calorimetry, precise lattice parameter measurements, anomalous X-ray and neutron diffraction, and in situ electrical measurements. The calorimetric results confirm the presence of a solid solution at high temperatures, but with a large enthalpy of mixing that exceeds the predicted value. Because Co<sub>3</sub>O<sub>4</sub> and Co<sub>2</sub>ZnO<sub>4</sub> have essentially identical lattice parameters, this energetic destabilization must arise from factors other than the strain energy resulting from size mismatch. Changes in Co<sup>3+</sup> spin states vs. temperature and zinc content are proposed to account for the positive excess enthalpy, and may also provide additional entropy to stabilize the solid solution at high temperature.

© 2012 Elsevier Inc. All rights reserved.

### 1. Introduction

Cobalt-based spinels have been widely investigated for their electrical, optical, and magnetic properties, with application in catalysts [1–3], batteries [4–6], sensors [7], pigments [8], and electrochromic [9] devices. While both Co<sub>3</sub>O<sub>4</sub> and Co<sub>2</sub>ZnO<sub>4</sub><sup>1</sup> have been studied for decades, interest in Co<sub>2</sub>ZnO<sub>4</sub> has increased recently, owing to its relationship to the new p-type transparent semiconductor Ir<sub>2</sub>ZnO<sub>4</sub> [10] and its application as a hole transport layer in organic photovoltaics [11]. The electrical, optical, and magnetic properties enabling these applications are related to the underlying thermodynamics governing the temperature-dependence of phase stability, cation arrangement, and spin states in these compounds. For example, the low temperature anti-ferromagnetism

of Co<sub>3</sub>O<sub>4</sub> (at  $T < \sim 40$  K) has been attributed to the tetrahedral Co<sup>2+</sup> ions, since octahedral Co<sup>3+</sup> in the low spin state has no unpaired electrons or magnetic moment [12,13]. Changes in cation distributions and spin states (e.g., with temperature or composition) could potentially change the magnetic properties, since, for example, high spin Co<sup>3+</sup> does have a magnetic moment. The site occupancy and spin state of Co is also relevant in the context of understanding the behavior of a related material, Co-substituted ZnO, which is considered a ferromagnetic “dilute magnetic semiconductor” [14], though the origins of such behavior remain under discussion. Also from an electrical perspective, cation distributions play a vital role, because the intrinsic p-type behavior of Co<sub>2</sub>ZnO<sub>4</sub> is caused by the presence of anti-site Zn on Co acceptor defects [15]. Of particular importance in the Co<sub>3</sub>O<sub>4</sub>–Co<sub>2</sub>ZnO<sub>4</sub> system is the question of whether a solid solution exists between the two end-member spinels, permitting tailoring of properties, in-depth studies of the roles of constituent cations and defects, and explanations for composition-dependent properties.

In general, solid solutions (alloys) of isovalent and isostructural compounds have positive enthalpies of mixing ( $\Delta H_{\text{mixing}}$ ). Examples include (III–V)–(III–V) or (II–VI)–(II–VI) alloys [16,17], oxide and halide solid solutions [18], and ternary chalcopyrites [19]. The mixing enthalpy generally scales with the size-mismatch between the constituents [18,19]. A few systems, usually with small size-mismatch, show zero or slightly negative heats of mixing

\* Correspondence to: 2220 Campus Drive, Evanston, IL 60208, U.S.A.

Fax: +1 847 491 7820.

E-mail address: [t-mason@northwestern.edu](mailto:t-mason@northwestern.edu) (T.O. Mason).

<sup>1</sup> Another widely used way of writing the spinel chemical formula is AB<sub>2</sub>O<sub>4</sub> (e.g., ZnCo<sub>2</sub>O<sub>4</sub>). We, however, write A<sub>2</sub>BO<sub>4</sub> (e.g., Co<sub>2</sub>ZnO<sub>4</sub>), which is common for spinels with formal cation valencies Z<sub>A</sub>=2 and Z<sub>B</sub>=4 such as Mg<sub>2</sub>TiO<sub>4</sub>. For a normal 3–2 spinel, A here refers to the octahedral sites and B to the tetrahedral sites. The main reason for our choice is the fact that the work presented here is part of a larger project that treats all A<sub>2</sub>BX<sub>4</sub> compounds (not only spinels) in different structure-types including olivine Fe<sub>2</sub>SiO<sub>4</sub>, β-K<sub>2</sub>SO<sub>4</sub> or La<sub>2</sub>CuO<sub>4</sub> for which A<sub>2</sub>BX<sub>4</sub> is the generally used notation.

[20, 21, 22]. When  $\Delta H_{\text{mixing}} > 0$ , the phase diagram exhibits a miscibility gap below some critical temperature ( $T_c$ ), and complete solid solution above. Thus, a positive heat of mixing is an indication of possible exsolution at low temperature, whereas a negative heat of mixing is suggestive of ordering.

The isovalent and isostructural system  $\text{Co}_3\text{O}_4$ – $\text{Co}_2\text{ZnO}_4$  is likely to show a small positive mixing enthalpy and the consequent existence of solid solution above a moderately low temperature and phase separation below. Both end-member spinels are nominally normal in cation distribution, with  $\text{Co}^{3+}$  on octahedral sites and  $\text{Zn}^{2+}$  and  $\text{Co}^{2+}$  on tetrahedral sites [23]. The ionic radii of  $\text{Zn}^{2+}$  and  $\text{Co}^{2+}$  in tetrahedral coordination are very similar (0.74 Å and 0.72 Å, respectively [24]), and the lattice parameters of the two end-members are virtually identical (e.g., 8.0837 Å at 23 °C for  $\text{Co}_3\text{O}_4$  from PDF card 01–080–1541 [25] and 8.0946 Å at 25 °C for  $\text{Co}_2\text{ZnO}_4$  from PDF card 00–23–1390 [26]). Thus one expects the mixing enthalpy to be small-positive. Not surprisingly, Robin [27] described  $\text{Co}_2\text{ZnO}_4$ – $\text{Co}_3\text{O}_4$  as a continuous solid solution in his very early phase diagram (though without extensive substantiation).

In spite of these observations, there is no conclusive experimental evidence to date for the existence of a solid solution. One of the challenges is related to the aforementioned similarity of the Zn and Co ionic radii. For example, Robin [27] noted the difficulty of quantitative measurements of composition from lattice parameters of equilibrated samples because the parameters varied so little across the supposed solid solution. In the present work we confirm that the lattice parameters of equilibrated compositions in the  $\text{Co}_3\text{O}_4$ – $\text{Co}_2\text{ZnO}_4$  join are virtually indistinguishable. It should be pointed out that our work is in contrast to that of Petrov et al. [28] on samples prepared at low temperature in potentially metastable structural states (see below). Thus the question of whether a complete solid solution exists under equilibrium conditions remains open.

In our recent theoretical efforts on the  $\text{Co}_3\text{O}_4$ – $\text{Co}_2\text{ZnO}_4$  system [23] we have calculated the energy needed to substitute a single Co-on-Zn (tetrahedral) anti-site defect in the 56 atom supercell of  $\text{Co}_2\text{ZnO}_4$  and a single Zn-on-Co (octahedral) anti-site defect in the same size supercell of  $\text{Co}_2\text{CoO}_4$  ( $\text{Co}_3\text{O}_4$ ), using first principles approaches. The calculated anti-site enthalpies of formation are  $< 0.05 \pm 0.1$  eV in either case, indicating a very small enthalpy of mixing in thermodynamic equilibrium. Straightforward calculation of the enthalpy of mixing ( $\Delta H_{\text{mixing}} = E[(\text{Co}_2\text{CoO}_4)_{0.125}(\text{Co}_2\text{ZnO}_4)_{0.875}] - 0.125E(\text{Co}_2\text{CoO}_4) - 0.875E(\text{Co}_2\text{ZnO}_4)$ ) yields a negligibly small value, consistent with the small anti-site formation energies. Accounting for entropy (owing to configurational contributions of arranging Co-on-Zn sites in  $\text{Co}_2\text{ZnO}_4$  and Zn-on-Co sites in  $\text{Co}_2\text{CoO}_4$ ) at higher temperatures resulted in the calculated phase diagram of

Fig. 1, showing continuous solid solution at high temperature, as evidenced by the overlap of the Zn-substituted  $\text{Co}_3\text{O}_4$  and Co-substituted  $\text{Co}_2\text{ZnO}_4$  boundaries.

The present work was undertaken to test our first-principles predictions regarding the  $\text{Co}_3\text{O}_4$ – $\text{Co}_2\text{ZnO}_4$  solid solution, in particular to provide experimental evidence for high temperature solid solution and to probe the thermodynamics of mixing in this system. To accomplish these tasks, we combined high temperature oxide melt solution calorimetric methods, differential scanning calorimetry, precise lattice parameter measurements (on quenched specimens), in situ electrical property measurements (conductivity, thermopower), and neutron and anomalous X-ray diffraction (on quenched specimens).

## 2. Experimental approach

### 2.1. Synthesis

The spinel phase(s) of the ZnO– $\text{Co}_3\text{O}_4$  system require synthesis at relatively low temperatures [27], so a low temperature aqueous processing route (decomposition of mixed nitrates) was chosen. This approach mixes cations at the atomic level in a much faster time frame than conventional solid state processing at low temperatures. The exact water contents of cobalt nitrate hexahydrate, 99.999%, and zinc nitrate hexahydrate, 99.998%, (both Alfa Aesar, Ward Hill, MA) were determined by measuring the weight loss of the nitrates upon heating to oxides in pre-dried crucibles. Then stoichiometric amounts of the Co and Zn nitrate hydrates were added to de-ionized water to yield nominal compositions  $\text{Co}_{3-x}\text{Zn}_x\text{O}_4$  in the range  $0 \leq x \leq 0.9$ . The nitrate solutions were stirred for approximately 8 h at 40–50 °C to mix the cations and evaporate most of the water. Then the concentrated solutions/gels were heated to 390 °C in a box furnace in a fume hood to remove residual water and nitrogen oxides, resulting in the formation of cobalt zinc oxide powders. Powders were ground with an agate mortar and pestle, pressed uniaxially at 125 MPa into pellets, sintered in air and quenched in air. Three sintering options were employed to fabricate samples with different phase compositions and cation ratios: 60 h at 800 °C (spinel phase(s) for  $0 \leq x \leq 0.72$  and spinel+wurtzite for  $x > 0.72$  [23]), 134 h at 600 °C followed by 96 h at 570 °C (spinel phase(s) for  $x=0.9$ ), and 134 h at 650 °C followed by 96 h at 570 °C (spinel phase(s) for  $x=0.75$ ). During sintering, the pellets were nested inside three crucibles within a bed of sacrificial powder of the same composition, to minimize both contamination and cation volatilization.

### 2.2. Sample characterization: Composition, microstructure, lattice parameters

Wavelength-dispersive X-ray fluorescence (XRF) with a Bruker S4 Pioneer spectrometer (Bruker AXS Inc, Madison, WI) was employed to verify the compositions of selected samples. To further analyze compositions as well as compositional homogeneity, electron probe microanalysis (EPMA) was also performed on every sample (15 points per sample) with a Cameca SX-100 electron microprobe (Cameca Instruments, Inc., Madison, WI). Sample densities were determined from measured masses and geometries and were found to be approximately 50% of the theoretical density. To determine average grain sizes, fracture surfaces were observed using a S4800 FE-SEM (Hitachi High-Technologies, Schaumburg, IL), and the resulting micrographs were analyzed with the program ImageJ to measure and determine the average of the apparent grain diameters. Phase verification was performed by X-ray diffraction (XRD) with Cu  $K_\alpha$  radiation over the  $2\theta$  range of 25–80° using a Scintag XDS2000 diffractometer (Scintag Inc, Cupertino, CA), a liquid  $\text{N}_2$ -cooled Ge

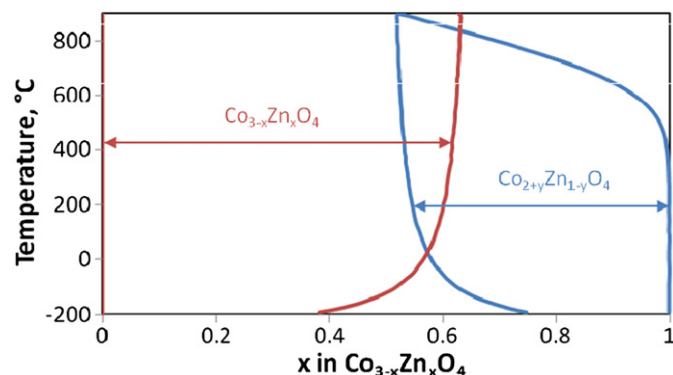


Fig. 1. Theoretical prediction of spinel ( $\text{Co}_{2+y}\text{Zn}_{1-y}\text{O}_4$  and  $\text{Co}_{3-x}\text{Zn}_x\text{O}_4$ ) stability regions (modified from Ref. [23]). The two regions overlap at high temperatures indicating the prediction of a complete solid solution.

detector (GLP-10195/07-S, EG&G ORTEC, Oak Ridge, TN), a step size of  $0.02^\circ$ , a dwell time of 1 s, a divergence slit of 2 mm, and a receiving slit of 0.5 mm. Lattice parameters were determined from subsequent XRD scans using Si powder (99.9995%, Sigma Aldrich) as an internal or external standard (both gave similar results) and the “whole pattern fitting” Rietveld refinement option (with fixed Si lattice parameter) in JADE 9 software. The lattice parameter of  $\text{Co}_{2.3}\text{Zn}_{0.7}\text{O}_4$  was also determined by neutron diffraction as described below.

### 2.3. Oxide melt solution calorimetry

High temperature oxide melt solution calorimetry was performed using instruments and techniques described previously [29,30]. Sample pellets ( $\sim 5$  mg) were dropped into a sodium molybdate ( $3\text{Na}_2\text{O}-4\text{MoO}_3$ ) melt (20 g) at  $700^\circ\text{C}$  in a platinum crucible in a custom built Calvet microcalorimeter. The final state was dissolved ZnO and CoO. Calibration used the heat content of alumina.

### 2.4. Anomalous X-ray diffraction and neutron diffraction

The distribution of A, B, and B' cations in an  $\text{A}_2\text{BO}_4-\text{A}_2\text{B}'\text{O}_4$  spinel solid solution is one factor contributing to the thermodynamics of mixing. For example, the magnitude of the ideal configurational entropy resulting from cation distributions is proportional to the number of sites involved in cation exchange going from one end-member to the other. In this work, the fractions of anti-site defects (Zn on octahedral sites and Co on tetrahedral sites) in selected bulk samples (quenched from  $800^\circ\text{C}$ ) were determined experimentally by anomalous X-ray diffraction (AXRD) on beamline 2-1 at the Stanford Synchrotron Radiation Lightsource, SLAC National Accelerator Laboratory. For the spinel structure, certain diffraction peaks correspond to scattering from different sublattices of octahedrally and tetrahedrally coordinated cations. Specifically, the (2 2 2) reflection probes only octahedral sites (Oh sites), whereas the (4 2 2) reflection probes only tetrahedral sites (Td sites). The intensity of these reflections was measured as we varied the energy of the incident X-ray through the *K* absorption edges of Co and Zn. The shape of the intensity vs. energy plot near a given element's edge indicates how much of that element populates the relevant site. Qualitatively, a large minimum in (2 2 2) peak (or (4 2 2) peak) intensity near the edge signals a large fraction of the Oh sites (or Td sites) is occupied by this specific element. Quantitatively, by using composition as a constraint and the fraction of site occupancy as variables, we fit the energy-dependent integrated peak intensities to simulated AXRD results. This allows us to determine the fraction of Oh and Td sites occupied by Co and Zn, and therefore the complete cation arrangement for a known composition. Further details of this approach, as applied to thin films of  $\text{Co}_2\text{ZnO}_4$ , are given in Ref. [31].

The neutron diffraction experiment was performed on the high-resolution BT-1 32 detector powder diffractometer at the NIST Center for Neutron Research (Gaithersburg, MD). A Cu ( $3\ 1\ 1$ ) monochromator with a  $90^\circ$  take-off angle, a wavelength of  $1.540\text{ \AA}$ , and in-pile collimation of 60 min of arc were used. Diffraction measurements were done over an angular range of  $2.8^\circ$  to  $162.8^\circ$  with a step size of  $0.05^\circ$ . The powder sample was loaded in a vanadium container and data were collected under ambient environment. Rietveld refinement of the neutron diffraction data was subsequently carried out using GSAS software with the EXPGUI interface [32] to determine the site occupancy and lattice parameter.

### 2.5. Differential scanning calorimetry (DSC)

DSC was conducted using a Setaram (Caluire, France) Labsys Evo thermal analyzer with a heat capacity sensor using  $380\ \mu\text{L}$  Pt crucibles with lids. Sample temperature calibration was performed by melting Sn, Ag, and Au standards in alumina crucibles.

### 2.6. Electrical Measurements

Equilibrium high temperature simultaneous conductivity and thermopower measurements were made in air in van der Pauw geometry on pellet samples using a custom-built sample holder, with type S thermocouples serving as the electrical contacts. Specimens were held to one side of the hot zone of a tube furnace to achieve the required  $\sim 10^\circ\text{C}$  thermal gradient for Seebeck measurements. Current reversal was employed to average out thermovoltage contributions to conductivity measurements. Porosity corrections were applied to determine conductivities corresponding to the dense phase, using the Bruggeman Symmetric model [33].

## 3. Results & discussion

### 3.1. Chemical/microstructural characterization

For the experimental study of phases formed, it was important to ensure that samples had large enough grains for any surface/grain boundary contributions to the measured enthalpies and conductivities to be negligible. Analysis of SEM micrographs confirmed that the average grain size for samples sintered at  $800^\circ\text{C}$  for 60 h was between  $0.4(\pm 0.2)\ \mu\text{m}$  and  $0.8(\pm 0.4)\ \mu\text{m}$ , depending on composition. Such grain sizes imply small grain boundary volume fractions (e.g., less than 4% for a hypothetical, conservative grain boundary width of 10 nm). Compositional accuracy and homogeneity were also verified from the XRF and EPMA results, shown in Table 1. Good agreement between target and measured compositions (overall Zn substitution level, *x* in  $\text{Co}_{3-x}\text{Zn}_x\text{O}_4$ , within 0–0.05 of the target value) was found. Since the size of the electron microprobe beam was larger than the average grain size, it was not possible to determine conclusively from the apparent spatial variation in measured composition values whether the samples were single phase or phase-separated; however, the variation in composition seen for individual analyses within a given sample ranged from 0.01 to 0.1 (in terms of *x*), with only very occasional grains showing variations greater than 0.05. This small variation suggests homogeneous (over the probe volume), rather than phase-separated samples, when they are prepared at high temperature. (By contrast, samples prepared by a similar route but at much lower temperatures were observed to be chemically inhomogeneous by EPMA, which could be indicative of phase separation at lower temperatures, although sluggish kinetics may also play a role.)

From XRD all the samples were confirmed to be cubic spinels, space group  $\text{Fd}\bar{3}\text{m}$ , with no wurtzite phase detected. The lattice parameters determined using the Si standard and Si PDF # 00–027–1402 are shown in Fig. 2 along with sample XRD patterns, for samples made at  $800^\circ\text{C}$  and measured at room temperature. Changes in the lattice parameter vs. composition are very slight; the value for  $\text{Co}_3\text{O}_4$  is  $8.0838 \pm 0.0004\ \text{\AA}$ , in good agreement with the reported value [25], and for  $\text{Co}_{2.3}\text{Zn}_{0.7}\text{O}_4$  (near the terminal solubility at  $800^\circ\text{C}$ ) it is  $8.0856 \pm 0.0004\ \text{\AA}$  by XRD and  $8.087 \pm 0.001\ \text{\AA}$  by neutron diffraction. Thus the lattice constant data neither prove nor disprove the presence of a solid solution.

**Table 1**  
Composition analysis, thermochemical data (heat of drop solution, heat of mixing, and heat of formation from CoO, ZnO plus O<sub>2</sub>, including estimates for Co<sub>2</sub>ZnO<sub>4</sub>), and in situ high temperature conductivity and thermopower values for selected samples.

Target composition, $x$ in Co <sub>3-x</sub> Zn <sub>x</sub> O <sub>4</sub>	Measured composition, $x$ , by microprobe (XRF)	Drop solution enthalpy in (kJ/mol) (drops made)	Enthalpy of formation from CoO, ZnO plus O <sub>2</sub> (kJ/mol)	Enthalpy of mixing (kJ/mol)	Electrical conductivity (S/cm) at 717.56 °C	Thermopower (μV/K) at 717.56 °C
0	0	271.05 ± 3.72 (8)	-211.55	0	11.82	+296.9
0.15	0.16 ± 0.02	264.29 ± 2.9 (8)	-204.54	5.81	5.74	+335.9
0.3	0.3 ± 0.1 (0.32)	259.28 ± 4.25 (7)	-199.31	9.99	5.14 <sup>a</sup>	+351.0 <sup>a</sup>
0.45	0.50 ± 0.07	260.28 ± 1.7 (9)	-200.00	7.79	2.46	
0.5	0.53 ± 0.04	257.50 ± 2.65 (8)	-197.17	10.39		
0.6	0.64 ± 0.07 (0.62)	260.53 ± 2.57 (11)	-200.30	6.71	1.71	+461.3
0.75		258.72 ± 3.06 (6)	-198.05	7.87		
0.9		262.80 ± 3.63 (7)	-201.90	2.89		
1		265.1 (estimate)	-204.04 (estimate)	0		

<sup>a</sup> The sample used for electrical measurements for this composition contained Mg as an intentional dopant, which did not appear to dramatically alter the high temperature behavior.

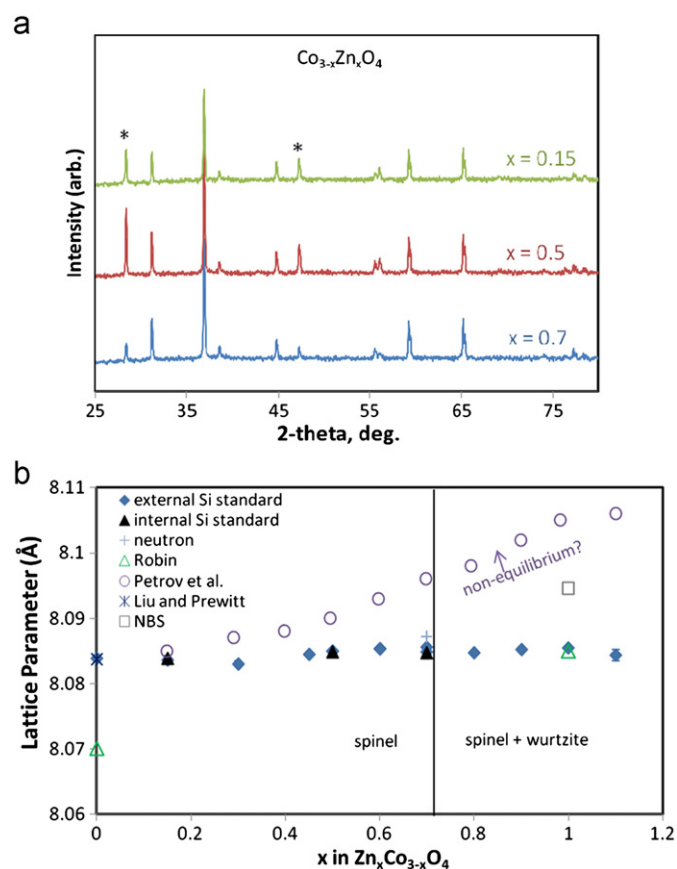


**Fig. 2.** (a) XRD patterns for selected samples. Asterisks mark Si peaks; all other peaks are spinel phase. (b) Lattice parameters vs. composition for samples quenched from 800 °C and measured at room temperature. The vertical line indicates the phase boundary at the synthesis temperature for the present study, while the data from Petrov et al. [28], Robin [27], the National Bureau of Standards (NBS) [26] and Liu and Prewitt [25] are all spinel phase.

### 3.2. Thermal analysis

In the differential scanning calorimetry measurements, shown in Fig. 3, both Co<sub>2.7</sub>Zn<sub>0.3</sub>O<sub>4</sub> and Co<sub>3</sub>O<sub>4</sub> show a strong endotherm with large weight loss above 900 °C; this is the reduction of cobalt to the divalent state. Co<sub>2.7</sub>Zn<sub>0.3</sub>O<sub>4</sub> decomposes (to divalent oxides) at a slightly lower temperature than Co<sub>3</sub>O<sub>4</sub>, which could indicate slight destabilization of the spinel with Zn incorporated, in agreement with the calorimetry results presented below. Because of the fast heating rate in the DSC measurements, the decomposition

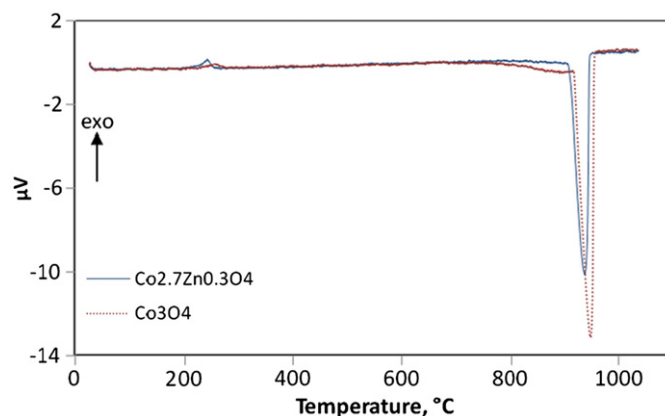


**Fig. 3.** DSC measurement for two spinel samples: pure Co<sub>3</sub>O<sub>4</sub> and Co<sub>2.7</sub>Zn<sub>0.3</sub>O<sub>4</sub>. In both spinels there is a small exothermic blip (less than 1 kJ/mol in magnitude) near 200 °C. It is not seen on cooling or in the second run, so it may be some relaxation of a metastable state (e.g., strain, quenched in disorder). Because it is so small it really is not important to energetics.

temperatures shown are higher than reported equilibrium values [34], even though the comparison between the two compositions is meaningful. Our electrical measurements (not shown) at a slower heating rate, 0.31–0.36 °C/min, agree well with the reported Co<sub>3</sub>O<sub>4</sub> decomposition temperature [34] (the onset of the conductivity drop is at 898 °C) and also exhibit a gradual decrease in decomposition temperature as more Zn is incorporated, down to 896 °C for  $x=0.45$  and 894 °C for the terminal spinel composition on the Zn side ( $x \approx 0.54$  in the spinel phase at the decomposition point). Thus the electrical data are in qualitative agreement with the DSC data and provide further support for the existence of a solid solution at these temperatures.

Co<sub>3</sub>O<sub>4</sub> also shows a more gradual and less intense endothermic peak in Fig. 3, without weight loss, starting about 730 °C, which is not seen in the zinc spinel. The lower temperature endotherm in Co<sub>3</sub>O<sub>4</sub> represents the low spin-to-high spin transition studied previously by a different scanning calorimetry technique by Mocala et al. [35]. Its absence in Co<sub>2.7</sub>Zn<sub>0.3</sub>O<sub>4</sub> is noteworthy. Zinc cobalt spinels have been suggested to contain mostly low spin Co<sup>3+</sup> at low temperatures [12, 36]. The absence of a transition before decomposition could be explained by several different scenarios: (1) If the spin transition moves to higher temperature with increasing zinc content, while the reduction of the spinel occurs at approximately the same temperature, the Co<sub>2.7</sub>Zn<sub>0.3</sub>O<sub>4</sub> may remain low spin until it decomposes. Then the degree of spin disorder at the synthesis temperature of our samples (800 °C) will diminish with increasing zinc content. (2) Spin disorder in

$\text{Co}_{2.7}\text{Zn}_{0.3}\text{O}_4$  might occur at lower temperature, with a smaller transition enthalpy (since the entropy would remain the same). If this transition is more spread out in temperature, it might not be detectable in the DSC scan. In this case the extent of spin disorder at the synthesis temperature would increase with zinc content. A lower temperature spin-unpairing transition for  $\text{Co}^{3+}$  in  $\text{Co}_2\text{ZnO}_4$  than in  $\text{Co}_3\text{O}_4$  has previously been suggested by Cossee [12] on the basis of magnetic measurements, where high temperature deviations from Curie–Weiss behavior began at lower temperatures in  $\text{Co}_2\text{ZnO}_4$  than in  $\text{Co}_3\text{O}_4$ . (3) A less likely scenario, since it is at variance with previous reports [12,36], is that even at room temperature, zinc-containing spinels contain exclusively high spin  $\text{Co}^{3+}$ . In this case also, the extent of spin disorder at synthesis temperature would increase with zinc content. More detailed studies are needed to distinguish among these possibilities, but are beyond the scope of the present work.

In  $\text{Co}_3\text{O}_4$  the endotherm related to the low spin-to-high spin transition appears smaller in magnitude than the peak seen by Mocala et al. [35] by step-scanning calorimetry at much slower heating rates. In both spinels studied, there is a small (less than 1 kJ/mol in magnitude) exotherm on heating near 200 °C, which is not seen on cooling or in second heating runs. This effect suggests the annealing of some metastable state, perhaps related to strain or spin state. These two observations may indicate that spin states equilibrate on a timescale of minutes on heating or cooling rather than instantaneously.

### 3.3. Anomalous X-ray diffraction

As mentioned previously, anomalous X-ray diffraction (AXRD) was employed to better understand the contribution of cation distributions to the thermodynamics of mixing. Fitting of AXRD diffraction data for samples quenched from 800 °C ( $x=0.3, 0.7$ ) showed negligible concentrations of Zn on octahedral sites (< 5% of the octahedral sites occupied by Zn), within experimental uncertainty. These results confirm the essentially normal distribution of cations across the solid solution, as shown in Fig. 4, i.e., the overall composition can be expressed as  $\text{Co}_2(\text{Zn}_x\text{Co}_{1-x})\text{O}_4$ , where the parentheses indicate the tetrahedral species. Our

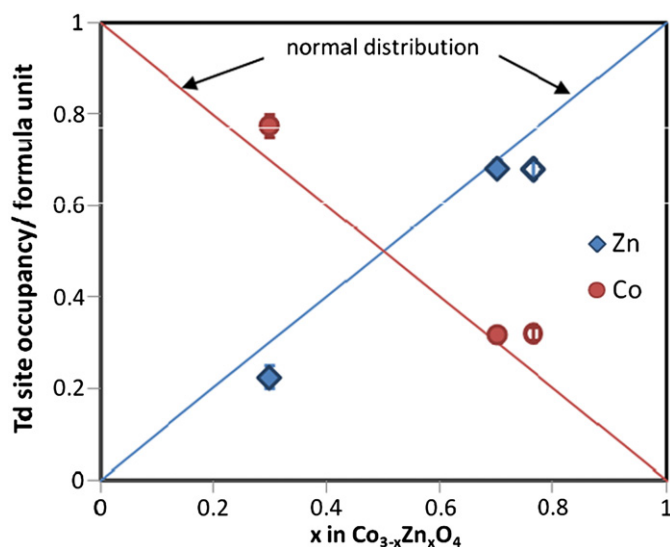


**Fig. 4.** AXRD (closed symbols) and neutron diffraction (open symbols) results for occupancy of the tetrahedral site by Zn and Co in bulk samples quenched from 800 °C and measured at room temperature. The vast majority of Zn ions occupy tetrahedral sites. (The composition of the neutron diffraction results reflects the value determined by fitting of neutron data without constraining the overall Zn:Co ratio.)

first-principles calculations also predicted very low concentrations of Zn on octahedral sites in equilibrium samples [23]. It should be mentioned that these particular AXRD measurements have not discriminated between  $\text{Co}^{2+}$  and  $\text{Co}^{3+}$  (nor between low- and high-spin  $\text{Co}^{3+}$ ). It has been suggested [25] that cation disordering in  $\text{Co}_3\text{O}_4$  may accompany the high temperature spin unpairing transition of  $\text{Co}^{3+}$ , and so some  $\text{Co}^{2+}$  occupancy of octahedral sites is possible in these samples quenched from 800 °C, particularly in compositions with lower Zn contents. Mocala et al. [35] argued that this disorder is limited to at most 5–10% of the octahedral Co sites being occupied by  $\text{Co}^{2+}$  once the transition is complete, while Chen et al. [34] calculated about 15% at the synthesis temperature. Overall, however, these spinels are mostly normal.

### 3.4. Enthalpies of mixing

Drop solution enthalpies for various compositions are plotted in Fig. 5 (error bars are two standard deviations of the mean). Instead of the linear behavior of a mechanical mixture (or of an ideal solution), a significant curvature in the enthalpies of drop solution is seen. This strongly suggests different chemical interactions at intermediate compositions than in a mechanical mixture of end-members and is strong evidence for the existence of a solid solution. A quadratic fit to the enthalpy of drop solution gives

$$\Delta H_{\text{drop solution}} = (270.10 \pm 1.72) - (38.07 \pm 7.54)x + (33.07 \pm 8.16)x^2 \text{ (kJ/mol)}$$

The enthalpy of drop solution of the end-member  $\text{Co}_2\text{ZnO}_4$  is estimated to be 265.10 kJ/mol. The quadratic term gives an interaction parameter,  $W$ , of  $33.07 \pm 8.16$  kJ/mol. Since the enthalpy of drop solution of the intermediate compositions is less endothermic than that of a mechanical mixture, it takes less energy to dissolve them, implying they are less stable and the interaction parameter is positive. The enthalpy of mixing is then given by

$$\Delta H_{\text{mixing}} = Wx(1-x)$$

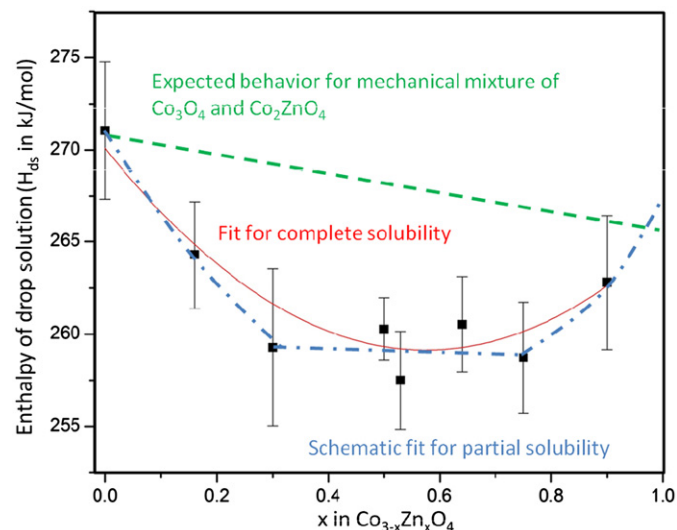


**Fig. 5.** Drop solution enthalpies for bulk samples of various compositions. Three possible “fits” are shown: a schematic linear fit (green dashed line) which would indicate an ideal solution or mechanical mixture, a quadratic fit (red solid line) which would indicate a complete solid solution, and a schematic combined fit (blue dotted and dashed line) which would indicate partial solubility with a small miscibility gap at this temperature. (For interpretation of the references to color in this figure legend, the reader is referred to the web version of this article.)

The magnitude of the interaction parameter is much larger than that expected from consideration of strain energy arising from ionic size mismatch or lattice parameter change alone [37], since these differences are very small in the present system.<sup>2</sup> If we consider the mixing entropy of the spinel solid solution to arise from the mixing of divalent Co and Zn on tetrahedral sites, then the system would show regular solution behavior, with the free energy of mixing given by

$$\Delta G_{\text{mixing}} = Wx(1-x) + RT[x\ln(x) + (1-x)\ln(1-x)]$$

The critical temperature for exsolution (the top of the solvus or immiscibility dome) would be given by

$$T_c = W/2R = 1989 \pm 491\text{K or } 1716 \pm 491^\circ\text{C}$$

Furthermore, based on the calculated solvus for this model, a maximum of 9.4 mol% of each end-member would be soluble in the other end-member at the synthesis temperature of 800 °C (using the smallest possible value for  $W$ ), which is at variance with the computational, microanalysis, and calorimetric observations.

The drop solution enthalpies could alternatively be interpreted to show a straight line segment separating two curved regions, as in the dashed curve of Fig. 5. Such an interpretation would be consistent with a small miscibility gap in the center of the  $\text{Co}_3\text{O}_4$ – $\text{Co}_2\text{ZnO}_4$  system, but not with the very large immiscibility implied by the regular solution model above. In contrast, the relatively high degree of homogeneity observed in the EPMA results argues in favor of complete solid solution rather than this small miscibility gap. Equilibrium electrical conductivity and thermopower measurements in the range 700–800 °C (see Table 1) also showed monotonic trends with composition, without discontinuities that might be expected to arise from phase separation at intermediate compositions. Further work is warranted to confirm the phase separation and solvus behavior at lower temperatures.

At 800 °C, the spinel phase does not extend all the way to  $\text{Co}_2\text{ZnO}_4$  (Fig. 1); for this composition, a more cobalt-rich spinel exists in equilibrium with a wurtzite (Co,Zn)O solid solution [23]. This retrograde solubility into the spinel does not imply any substantial destabilization in the spinel solid solution itself, but rather a more favorable free energy for the two-phase assemblage. We will analyze this equilibrium at both bulk and nano-scale in a future communication.

We conclude that the thermodynamics of mixing in this system is more complex than a simple regular solution and seek structural explanations for both the surprisingly large positive enthalpy of mixing and the observed large solid solubility.

### 3.5. Cation distributions, spin states, and thermodynamic complexity

The large positive heats of mixing in the present work appear to be at variance with the observed solid solution formation and exceed considerably the values calculated from first principles. One possible resolution would be the existence of additional thermodynamic contributions, e.g., additional sources of entropy that lower the free energy and/or additional sources of mixing enthalpy that vary strongly with temperature, becoming less positive at higher temperature. Here we seek possible sources of such behavior.

<sup>2</sup> O'Neill and Navrotsky [27] derived an empirical relationship between the interaction parameter ( $W$ ) and the difference in cation radii for the case of 3+ cations exchanging in spinel solid solutions, where  $W$  is negligible for small radii differences. While no relationship was determined for 2+ cation exchange, as in the present case, those authors suggested that  $W$  should also be negligible for cases of similar 2+ cation radii. (Note that the values of  $W$  for  $\text{Co}_3\text{O}_4$ – $\text{M}_2\text{CoO}_4$  systems deviate from the trend unless the ionic radius of high spin (rather than low spin)  $\text{Co}^{3+}$  is used.)

Changes in spin state with temperature and composition could contribute to the entropy and/or temperature dependence of the enthalpy of mixing. Mocala et al. [35] studied the spin unpairing transition in  $\text{Co}_3\text{O}_4$ , which occurs over a temperature range starting near 725 °C and is interrupted, before completion, by decomposition to CoO. They estimated an enthalpy of  $53 \pm 4$  kJ/mol and an entropy of  $46 \pm 4$  J/(mol K) for the complete transition, with that entropy value in good agreement with the theoretical value of  $2R\ln 15$  for the unpairing of two moles of spins. At 800 °C, the temperature of sample synthesis in our experiments, the transition is only partially complete, with only about 10% of the total entropy attained (based on the data of Mocala et al. [35]). In our  $\text{Co}_3\text{O}_4$  DSC data there is a slight indication of the onset of the spin transition, as seen by Mocala et al. [35], before decomposition, as a spread-out endothermic bump prior to the sharp decomposition reaction. In the Zn spinel, the baseline is flat right up to decomposition. If the transition is energetically less costly with increasing zinc substitution, it will move to lower temperature, resulting in more spin disorder in the solid solution at a given temperature. Thus the enthalpy and entropy of the solid solution may have additional terms resulting from such temperature- and composition-dependent disordering. The drop solution calorimetric data refer to samples cooled to room temperature. Presumably their spin state is largely or entirely low spin, but, if the energy of spin disordering depends in a complex way on composition, it may contribute to the observed heat of mixing. At present there is not enough information about spin state as a function of temperature, composition, and cooling/heating scenario to attempt a quantitative model. The salient point is that the enthalpy and entropy changes associated with spin disorder are potentially large enough to affect the thermodynamics of mixing.

## 4. Conclusions

High temperature calorimetric and electrical property studies of bulk, equilibrium  $\text{Co}_{3-x}\text{Zn}_x\text{O}_4$  ( $0 \leq x \leq 0.9$ ) have confirmed the first-principles theoretical prediction that a solid solution exists in the spinel phase at 800 °C. The large mixing enthalpy, however, is in disagreement with the small value predicted by first-principles calculations. Furthermore, it cannot be explained by considerations of cation anti-site concentrations or strain effects alone, since these are both small in the present system (as verified by anomalous X-ray diffraction studies, neutron diffraction studies, and Rietveld analysis of lattice parameter changes on quenched specimens). Instead, changes in the spin state of  $\text{Co}^{3+}$  as a function of Zn content and/or temperature are proposed as being responsible for additional contributions to the measured mixing enthalpy and/or large mixing entropy that stabilizes the solid solution at high temperatures. Evidence for changes in spin state with temperature and composition was seen in the differential scanning calorimetry behavior of  $\text{Co}_3\text{O}_4$  vs. that of  $\text{Co}_{2.7}\text{Zn}_{0.3}\text{O}_4$ . Further work is required to determine the exact location of the solvus and to quantify the origin of the anomalously large factors associated with the solution thermodynamics, e.g., to what extent spin states vary with temperature and composition, and the role they play in the thermodynamics of mixing.

## Acknowledgments

This work was supported by the "Center for Inverse Design," an Energy Frontier Research Center funded by the Office of Basic Energy Sciences, U.S. Department of Energy, under Grant No. DE-AC36-08G028308. CM and AN acknowledge funding from DOE Basic Energy Sciences grant DE-FG02-05ER15667. The X-ray

diffraction work was conducted in the J. B. Cohen X-Ray Diffraction Facility supported by the MRSEC program of the National Science Foundation (Grant No. DMR-0520513) at the Materials Research Center of Northwestern University. The anomalous X-ray diffraction work was carried out at the Stanford Synchrotron Radiation Lightsource, a national user facility operated by Stanford University on behalf of the U.S. Department of Energy, Office of Basic Energy Sciences. We acknowledge the support of the National Institute of Standards and Technology, U. S. Department of Commerce, in providing the neutron research facilities used in this work. YS, JSB, and MFT are grateful to Dr. Mark Green for his help with data collection and discussion about data refinement.

## References

- [1] K. Omata, T. Takada, S. Kasahara, M. Yamada, *Appl. Catal., A* 146 (1996) 255–267.
- [2] P. Nkeng, J.-F. Koenig, J.L. Gautier, P. Chartier, G. Poillerat, *J. Electroanal. Chem.* 402 (1996) 81–89.
- [3] M.M. Natile, A. Glisenti, *Chem. Mater.* 14 (2002) 3090–3099.
- [4] R.J. Gummow, D.C. Liles, M.M. Thackeray, *Mater. Res. Bull.* 28 (1993) 235–246.
- [5] W.J. King, A.C.C. Tseung, *Electrochim. Acta.* 19 (8) (1974) 485–491.
- [6] C. Ai, M. Yin, C. Wang, J. Sun, *J. Mater. Sci.* 39 (2004) 1077–1079.
- [7] A.-M. Cao, J.-S. Hu, H.-P. Liang, W.-G. Song, L.-J. Wan, X.-L. He, X.-G. Gao, S.-H. Xia, *J. Phys. Chem. B* 110 (32) (2006) 15858–15863.
- [8] C. Lin, Y. Li, M. Yu, P. Yang, J. Lin, *Adv. Funct. Mater.* 17 (2007) 1459–1465.
- [9] T. Maruyama, S. Arai, *J. Electrochem. Soc.* 143 (4) (1996) 1383–1386.
- [10] M. Dekkers, G. Rijnders, D.H.A. Blank, *Appl. Phys. Lett.* 90 (2007) 021903.
- [11] A. Zakutayev, J.D. Perkins, P.A. Parilla, N.E. Widjonarko, A.K. Sigdel, J.J. Berry, D.S. Ginley, *MRS Commun.* (2011) 23–26.
- [12] P. Cossee, *Recueil des Travaux Chimiques des Pays-Bas* 75 (1956) 1089–1096.
- [13] P. Dutta, M.S. Seehra, S. Thota, J. Kumar, *J. Phys. Condens. Matter* 20 (2008) 015218.
- [14] K. Samanta, P. Bhattacharya, R.S. Katiyar, W. Iwamoto, P.G. Pagliuso, C. Rettori, *Phys. Rev. B* 73 (2006) 245213.
- [15] J.D. Perkins, T.R. Paudel, A. Zakutayev, P.F. Ndione, P.A. Parilla, D.L. Young, S. Lany, D.S. Ginley, A. Zunger, N.H. Perry, Y. Tang, M. Grayson, T.O. Mason, J.S. Bettinger, Y. Shi, M.F. Toney, *Phys. Rev. B* 84 (2011) 205207.
- [16] G.B. Stringfellow, *J. Cryst. Growth* 27 (1974) 21.
- [17] A. Zunger, S. Mahajan, *Handbook of Semiconductors* 3B (1994) 1399.
- [18] P.K. Davies, A.N. Navrotsky, *J. Solid State Chem.* 46 (1983) 1.
- [19] S.B. Zhang, S.H. Wei, A. Zunger, *J. Appl. Phys.* 83 (1998) 3192.
- [20] P.K. Davies, A. Navrotsky, *J. Solid State Chem.* 38 (1981) 264.
- [21] R.G. Dandrea, J.E. Bernard, S.H. Wei, A. Zunger, *Phys. Rev. Lett.* 64 (1990) 36.
- [22] X.W. Zhang, G. Trimarchi, M. d’Avezac, A. Zunger, *Phys. Rev. B* 24 (2009) 241202.
- [23] T.R. Paudel, S. Lany, M. d’Avezac, A. Zunger, N.H. Perry, A.R. Nagaraja, T.O. Mason, J.S. Bettinger, Y. Shi, M.F. Toney, *Phys. Rev. B* 84 (2011) 064109.
- [24] R.D. Shannon, *Acta Crystallogr.* A32 (1976) 751–767.
- [25] X. Liu, C.T. Prewitt, *Phys. Chem. Miner.* 17 (1990) 168.
- [26] *Natl. Bur. Stand. (U.S.) Monogr.* 25 v. 10 (1972) 60.
- [27] J. Robin, *Ann. de Chim. (Paris)* 12 (10) (1955).
- [28] K. Petrov, L. Markov, R. Ioncheva, *J. Mater. Sci. Lett.* 4 (1985) 711–714.
- [29] A. Navrotsky, *Phys. Chem. Miner.* 24 (1997) 222.
- [30] S.V. Ushakov, A. Navrotsky, *Appl. Phys. Lett.* 87 (2005) 164103.
- [31] Y. Shi, P.F. Ndione, A. Zakutayev, J.S. Bettinger, N.H. Perry, P.A. Parilla, J.D. Perkins, T.O. Mason, D.S. Ginley, M.F. Toney. Biaxially textured spinel oxide films synthesized by pulsed laser deposition: site occupancy and conductivity, *Phys. Rev. B*, in preparation.
- [32] B.H. Toby, *Journal of Applied Crystallography* 34 (2001) 210–213.
- [33] D.S. McLachlan, M. Blaszkiewicz, R.E. Newnham, *J. Am. Ceram. Soc.* 73 (8) (1990) 2187–2203.
- [34] M. Chen, B. Hallstedt, L.J. Gauckler, *J. Phase Equilib.* 24 (3) (2003) 212–227.
- [35] K. Mocala, A. Navrotsky, D.M. Sherman, *Phys. Chem. Miner.* 19 (1992) 88–95.
- [36] F.K. Lotgering, *Philips Res. Rep.* 11 (1956) 337.
- [37] H.S.C. O’Neill, A. Navrotsky, *Am. Mineral.* 69 (1984) 733–753.